A Calcium Zirconate Based Combined Material for Calcium-Copper Chemical Looping Technology

Alexander Westbye[1,2*], Asunción Aranda[1], Pascal D. C. Dietzel[2], Luca Di Felice[1]

[1] Institute for Energy Technology (IFE), Department of Environmental Technology, Instituttveien 18, P.O. Box 40, 2007 Kjeller, Norway
[2] University of Bergen, Department of Chemistry, 7803 Bergen, Norway

[*] Corresponding author Alexander.Westbye@ife.no, mob.: + 47 977 59 398, Institute for Energy Technology (IFE), Instituttveien 18, P.O. Box 40, 2007 Kjeller, Norway.

Abstract

Combined calcium-copper materials based on calcium zirconate ($CaO/CuO/CaZrO_3$) for Calcium-Copper Chemical Looping (Ca-Cu Looping) have been synthesized using a scalable wet chemical method and characterized by powder X-ray diffraction (PXRD) with Rietveld refinement, temperature-programmed reduction (H_2-TPR) and oxidation (O_2-TPO), scanning electron microscopy (SEM), energy dispersive X-ray spectroscopy (EDS) and 45 - 50 cycles in a thermogravimetric analyser (TGA) representing realistic Ca-Cu Looping conditions. A material at 50 wt% active CuO loading and a CuO/CaO weight ratio of 2 deactivated due to copper migration and agglomeration, while materials with 40 wt% active CuO loading were stable throughout TGA cycles at CuO/CaO ratios of 2 and 10. 40 wt% CuO loaded combined $CaO/CuO/CaZrO_3$ materials are promising candidates for Ca-Cu Looping with a demonstrated tuneable and stable CuO/CaO ratio (≥ 2 [wt/wt]) that could lead to process intensification. The maximum CuO loading for the investigated materials is likely found in the range of [40, 50) wt%, subject to the constraints of Ca-Cu Looping relevant CuO/CaO ratios (≥ 2 [wt/wt]) and the performed TGA testing.

Keywords: Ca-Cu Looping, Combined Materials, Hydrogen Production, CO_2 Capture, CaO sorbent, Cu Oxygen Carrier.

1. Introduction

In 2010 the research group of Abanades et al. (Abanades et al., 2010) proposed the idea of Calcium-Copper Chemical Looping Combustion (Ca-Cu Looping), a flexible processing concept based on high temperature solids looping for power and/or hydrogen production (J. Fernández and Abanades, 2017). Ca-Cu Looping merges Calcium Looping (CaL) (P. Fennell, B. Anthony, 2015) and Chemical Looping Combustion (CLC) (Lyon and Cole, 2000) (Li et al., 2017a), utilizing a calcium oxide (CaO) based carbon dioxide (CO_2) sorbent and a copper-based oxygen carrier for efficient conversion of carbonaceous fuel with CO_2 capture. The concept has been further developed by the same group into a system of fixed bed reactors operating in parallel that could also be incorporated in an ammonia production plant (Fernández et al., 2012) (J. R. Fernández and Abanades, 2017) (Martínez et al., 2017). A 2018 techno-economical assessment compared Ca-Cu Looping with a typical fired tubular reformer reforming plant with amine capture and provided favourable results for Ca-Cu Looping (Martínez et al., 2019). However, the high processing temperatures (≤ 900°C) and harsh operating conditions (reducing gases, high pressure, steam etc.) in the Ca-Cu Looping process places substantial demands on materials performance. Materials development is a current bottleneck for the process, though the calcination step

has been demonstrated at TRL 4 (Fernández et al., 2018) and materials testing is currently being performed in fixed bed reactors at the 80 - 100 gram scale (L. Díez-Martín et al., 2018b). Still, the need for further materials development is crucial for the success of Ca-Cu Looping as a viable processing concept. In this work, a calcium-copper material based on calcium zirconate ($CaZrO_3$) has been characterized and tested as a potential candidate for Ca-Cu Looping.

Ca-Cu Looping utilizes three main processing steps in order to achieve hydrogen production from natural gas with CO_2 capture: (1) Sorption Enhanced Reforming (SER) (Martínez et al., 2013) (Fernandez et al., 2012) (2) copper (Cu) oxidation and (3) coupled calcium carbonate ($CaCO_3$) calcination and copper(II) oxide (CuO) reduction. In-depth discussions on process conditions for each step and reaction equations are thoroughly discussed elsewhere (Abanades et al., 2010) (Fernández et al., 2012) (J. R. Fernández and Abanades, 2017) (Martínez et al., 2017) (Martínez et al., 2019) and only a brief overview will be given here.

In the SER step, natural gas and steam (e.g. 1.0 – 2.5 MPa, 650°C, 2.5 kg_{CH4} kg_{cat}^{-1} h^{-1} (L. Díez-Martín et al., 2018b)) are reacted over a catalyst (e.g. a Ni/Al_2O_3 catalyst (Navarro et al., 2017)) to produce high purity hydrogen while capturing evolved CO_2 through exothermic CaO carbonation ($CaO(s) + CO_2(g) \rightarrow CaCO_3(s)$, $\Delta_r H^\circ_{298}$ = - 178.8 kJ mol^{-1}). The materials in the reactor after the SER step is in a $Cu/CaCO_3$ state. After the SER, an oxidation step is implemented where diluted air (5 vol% O_2) oxidizes the elemental copper to copper(II) oxide. In the following calcination step, a reducing gas composed of $CO/CH_4/H_2$ is used for exothermic copper(II) oxide reduction that drives the endothermic $CaCO_3$ calcination. The $CuO/CaCO_3$ material is thus reduced and calcined to Cu/CaO and the SER step can again be initiated. The theoretical CuO/CaO ratios required to drive the calcination to completion are in the range 1.8 – 4.4 [wt/wt] (1.3 – 3.1 [mol/mol]) (Abanades et al., 2010) (Fernández et al., 2012). The ratio primarily depends on the reducing gas available in the process, process heat integration and flow conditions. Ratios around 2.8 [wt/wt] (2.0 [mol/mol]) are typically implemented in Ca-Cu Looping process modelling (J. R. Fernández and Abanades, 2017).

Generally speaking there are many potential options for solid CO_2 sorbents: metal-organic frameworks (MOFs) (Pato-Doldán et al., 2017), alkaline ceramics (e.g. lithium zirconate, Li_2ZrO_3 (Xiao et al., 2011)), zeolites (Chen et al., 2014), silicate (Vieira and Pastore, 2014) etc. One of the most studied solid CO_2 sorbents is calcium oxide, usually supported by aluminium (Al), magnesium (Mg) and zirconium (Zr) oxides (Shokrollahi Yancheshmeh et al., 2016). The emphasis on CaO relative to the other sorbent options has mainly been low CaO cost and availability combined with a sufficiently high sorption / desorption (carbonation / calcination) reactivity, a high potential CO_2 carrying capacity (~0.784 $gCO_2/gCaO$) and low health risk (P. Fennell, B. Anthony, 2015) (Shokrollahi Yancheshmeh et al., 2016) (Valverde, 2013). The drawback of using CaO directly as e.g. natural limestone is its proneness to sintering and significant loss of CO_2 carrying capacity at elevated temperature through several carbonation / calcination cycles (Wang et al., 2010) (C. Wang et al., 2014). Sintering of CaO is an issue for the transient CO_2 capture capacity of these sorbents since calcination of CaO requires high temperatures (~900°C under 1.0 bar CO_2 (Valverde and Medina, 2015) (Baker, 1962)). Therefore, Al, Mg or Zr are often incorporated along with CaO in order to stabilize the sorbent.

Of special interest to the current work is the Ca/Zr sorbent system. ZrO_2 has a high Tammann temperature of 1221°C and several studies of CaO doping has set Zr forth as the best CaO dopant along with Al (Lu et al., 2009) (Radfarnia and Iliuta, 2013) (Al-based sorbent alternatives, e.g. mayenite ($Ca_{12}Al_{14}O_{33}$) and other calcium aluminates will not be discussed here - more thorough information on these materials is found elsewhere (Shokrollahi Yancheshmeh et al., 2016) (Lee and Park, 2015) (Kazi et al., 2017) (Zhou et al., 2012) (Luo et al., 2015)). Combining Zr and Ca for sorbent preparation has been investigated to some extent through e.g. flame spray pyrolysis (Lu et al., 2009), the sol-gel method (Broda and Müller, 2014), co-precipitation (Reddy et al., 2014), deposition-precipitation (Reddy et al., 2014) and wet chemical mixing (Zhao et al., 2014). The optimum Zr/Ca molar ratio in these studies range from 0.1 - 0.5, where *optimal* generally represents the highest stable CaO activity

obtainable without observing transient loss of CO_2 carrying capacity across implemented testing cycles. It seems evident that the stability of the capture capacity increases and the sorption capacity decreases as the Zr content is increased. In this work, the sorbent function of the calcium-copper material will be supported by $CaZrO_3$ (Tammann temperature of 1036°C), its formation promoted by adding Zr as a limiting reactant and implementing appropriate calcination conditions. $CaZrO_3$ is thermodynamically favourable > 610°C (Kalinkin et al., 2012).

Similar to CaO, Cu materials have been an active area of research in relation to high temperature solid looping technologies, e.g. CLC and Chemical Looping with Oxygen Uncoupling (CLOU) (Imtiaz et al., 2013). The low Tammann temperatures of Cu (405°C) and CuO (526°C) imply that copper-based oxygen carriers are prone to sintering and agglomeration at high temperature and that support structures and/or doping is required. Common choices for improving copper based oxygen carriers are other pure or mixed metal oxides, e.g. Al_2O_3 (Chuang et al., 2008) (L. Díez-Martín et al., 2018a), $MgAl_2O_4$ (Arjmand et al., 2012) or ZrO_2. Of special interest for this work are the reported Cu/Zr systems. Cu/Zr oxygen carriers have been prepared through freeze granulation (40/60 wt% CuO/ZrO_2) (Mattisson et al., 2009), aqueous paste preparation (mixing) (Adánez et al., 2004), co-precipitation (Laura Díez-Martín et al., 2018), doping through sol-gel combustion (2 – 10 wt% Zr) (Wang et al., 2015) and mechanical mixing (60/40 wt% CuO/ZrO_2) (K. Wang et al., 2014). The performance of the Cu/Zr materials are promising though the scalability of e.g. freeze granulation and sol-gel combustion are hurdles that must be overcome for large scale deployment. In the case of reported co-precipitation methods, Cu/Al_2O_3 systems seem favourable relative to Cu/Zr due to formation of monoclinic ZrO_2 that causes a poorer dispersion of Cu and Zr in the material (Laura Díez-Martín et al., 2018). A drawback of Cu/Al systems can on the other hand be strong Cu-support interactions that can result in reduced carrying capacities (i.e. $CuAl_2O_3$ formation (Imtiaz et al., 2013)). As observed for CaO materials, intimate contact between reactants during mixing / synthesis before calcination seem to be an important parameter for material stability.

A general point on CaO sorbents and Cu oxygen carriers is that direct comparisons between materials is made difficult by varying testing conditions used by different research groups (times on stream, metal loadings, carbonation / oxidation / reduction / calcination step order, cycling temperature as well as gas composition). TGA conditions for sorbent testing are more thoroughly discussed by F. Donat et al. (Donat and Müller, 2018) and J. Valverde (Valverde, 2013). Tables reporting collections of sorbent carbonation / calcination conditions can be found in papers by M. Zhao et al. (Zhao et al., 2014) and a review article by M. Shokrollahi et al. [10]. For oxygen carrier testing, Li et al. 2017 is recommended (Li et al., 2017b). Due to differences in test conditions it is not a straightforward task to identify state-of-the art materials for Ca-Cu Looping. Realistic current segregated materials (i.e. separate CaO and CuO particles) set-ups are likely in the 60 - 70 wt% CuO loading range and 25 – 32 wt% active CaO sorbent range (20 – 25 gCO_2/100g residual sorbent capture capacity).

Combined materials are an alternative approach to Ca-Cu Looping where Ca and Cu functions are incorporated into a single powder / particle. Possible advantages are process intensification through a higher potential active metal loading per reactor volume, avoidance of local overheating in copper particles (Qin et al., 2015) and better thermal contact between CuO reduction and $CaCO_3$ calcination during the Ca-Cu Looping calcination step. A potential downside to combined materials is that the CuO/CaO ratio must be fixed during synthesis.

Combined calcium-copper materials for Ca-Cu Looping are a fairly recent area of materials research though some interesting work has already been published. The simplest procedures include mixing of lime, CuO powder and calcium aluminate cement (Manovic and Anthony, 2011) (45/45/10 wt% $CaO/CuO/Al_2O_3$, steam used during TGA testing, 600 - 800°C TGA temperature) and e.g. core-in-shell approaches mixing cement, lime and CuO (Manovic et al., 2011) (≥ 50 wt% CuO, ≤ 40 wt% CaO particle configurations, steam used during TGA testing, 600 - 800°C TGA temperature). Loss of CO_2 capacity has been observed in these cement-based materials. Kierzkowska et al. have prepared a co-precipitated combined material (CuO/CaO molar ratios of 1.0, 1.3 and 3.3, no support structure) (Kierzkowska and

Müller, 2012) and a sol-gel derived combined material exploring Mg, Al and Mg-Al oxides as support (CuO/CaO molar ratios of 1.3 and 3.3, CuO content in the range 72.3 – 46.9 wt%) (Kierzkowska and Müller, 2013). These materials were tested at 750°C in a TGA without steam. Loss of transient CO_2 capture capacity was also observed for these materials. A CaO/CuO/MgO material has been prepared through wet mixing (11.2/63.8/25.0 wt% CaO/CuO/MgO, no steam used during TGA testing, 600 – 950°C TGA temperature) (Qin et al., 2012). The CO_2 capacity was shown to decline in TGA tests, likely due to "wrapping" of the sorbent by migrating Cu. Recently, J. Ma et al. have demonstrated a self-assembly template synthesis (SATS) for a core-shell structured MgO-Al_2O_3 supported calcium-copper material (no steam used during TGA testing, 750°C TGA temperature) (Ma et al., 2019) while J. Chen et al. have presented a solution combustion synthesis (SCS) (no support structure, no steam used during TGA testing, 650 - 800°C TGA temperature) (Chen et al., 2018) and a one-pot synthesis of hollow microspheres (no support structure, no steam used during TGA testing, 650 - 800°C TGA temperature) (Chen et al., 2019) showing promising results during cyclic TGA testing.

Another work of note is that of Qin et al. (Qin et al., 2013) where thermal pre-treatment (e.g. high calcination temperatures) and the effect of steam on combined particles were investigated. It was found that high calcination temperature and steam seamed to improve sorbent function. Our group have recently reported a mayenite based CaO/CuO/$Ca_{12}Al_{14}O_{33}$ material (CuO/CaO = 2.0 [wt/wt]) prepared using a hydrothermal synthesis route (Westbye et al., 2018)**.** It was found that 50 wt% CuO loaded materials lost oxygen carrying capacity regardless of CuO precursors while 40 wt% materials all showed stable cyclic TGA behaviour across 40 cycles for both CaO and Cu phases (steam used during TGA testing, 650 – 870°C TGA temperatures).

Developing and understanding the properties of combined materials is a promising driver for process intensification for Ca-Cu Looping and by extension hydrogen/power production from natural gas with CO_2 capture. This work follows the previous study on combined mayenite materials, and the main rationale for testing calcium-copper materials based on calcium zirconate is the higher Tammann temperature of the $CaZrO_3$ support that might improve the stability of the copper phase. By utilizing the same testing conditions and equipment as those employed for the mayenite material, the effect of the support structure on combined materials behaviour can be assessed.

In this work, a CaO/$CaZrO_3$ sorbent system reported by Zhao et al. (Zhao et al., 2014) has been modified and copper hydroxide ($Cu(OH)_2$) has been introduced in the modified procedure as a CuO precursor. Two materials at 40 and 50 wt% CuO loading have been prepared using a CuO/CaO = 2.0 [wt/wt] (1.4 [mol/mol]) and one material at 40 wt% CuO loading using a CuO/CaO = 10.0 (7.0 [mol/mol]) ratio. These loadings and ratios have been chosen as it is unlikely that a CuO/CaO ratio lower than 2.0 or higher than 10.0 is required for Ca-Cu Looping. Prepared materials have been subjected to various characterization techniques and 45 - 50 cyclic thermogravimetric analysis (TGA) cycles representing Ca-Cu Looping process conditions in order to assess the transient stability of the O_2 and CO_2 carrying capacities as well as material behaviour. To the authors knowledge, this work is the first to report a material using a $CaZrO_3$ support structure for combined calcium-copper materials.

2. Materials and Methods

2.1 Preparation of Materials

The preparation of CaO/CuO/$CaZrO_3$ materials is based on a wet chemical method for CaO/$CaZrO_3$ sorbent synthesis reported by M. Zhao et al. (Zhao et al., 2014). The method has been modified by introducing a copper(II) oxide precursor and by substituting ammonium hydroxide (NH_4OH)

with sodium carbonate (Na_2CO_3, > 99.5 % anhydrous, Merck) in the making of an aqueous pH = 11.0 solution. This change avoids the formation of a copper-ammonia complex (e.g. tetraamminecopper(II) cations, $[Cu(NH_3)_4]^{2+}$) that prevents precipitation of the Cu species. Copper hydroxide ($Cu(OH)_2$, technical grade, Sigma-Aldrich), calcium hydroxide ($Ca(OH)_2$, > 99%, Merck), zirconium(IV) oxynitrate hydrate ($ZrO(NO_3)_2 \cdot xH_2O$, 99%, Sigma-Aldrich), ethanol (EtOH, 96%) and deionized water were used in the described procedure. A 10.0 mmol Zr basis was selected, resulting in 3.0 – 6.5 g of product (calcined and oxidized) depending on the desired CuO loading and selected CuO/CaO ratio.

$Cu(OH)_2$ as-received and dried (> 48 h, 110°C) $Ca(OH)_2$ were weighed in stoichiometric amounts equivalent to a chosen theoretical composition of a calcined and oxidized product ($CaO/CuO/CaZrO_3$). $Ca(OH)_2$ and $Cu(OH)_2$ were mixed together under stirring in EtOH (2.0 mL EtOH $mmol^{-1}$ of Ca and Cu). The resulting suspension was transferred dropwise to a pH = 11.0 Na_2CO_3 (aq) solution (2.0 mL $mmol^{-1}$ of Ca and Cu) while being vigorously stirred.

Dried (> 48 h, 110°C) $ZrO(NO_3)_2 \bullet xH_2O$ was mixed in EtOH (5.0 mL $mmol^{-1}$ of Zr) in a separate beaker. The resulting suspension was added to a pH = 11.0 Na_2CO_3 (aq) solution (5.0 mL $mmol^{-1}$ of Zr) under stirring. In a final mixing step, the zirconium suspension was transferred dropwise to the calcium-copper suspension under vigorous stirring. The system was stirred for 30 min, left to settle for 3 h at ambient conditions, dried overnight (16 h, 110°C) and calcined at 950°C (1 h, 5°C min^{-1} heating rate).

Materials presented in this work are labelled as "CuO*x*_R*y*_T*z*", where *x* represents the theoretical CuO loading in weight percent (wt%), *y* denotes the CuO/CaO [wt/wt] mass ratio and *z* is the number of TGA cycles the material has been subjected to. A 40 wt% CuO loaded material prepared with a CuO/CaO ratio of 2.0 [wt/wt] subjected to 50 TGA cycles is thus CuO40_R2_T50. The three materials presented are CuO40_R2, CuO50_R2 and CuO40_R10.

2.2 Materials Characterization

Materials were characterized using powder X-ray diffraction (PXRD) and Rietveld refinement, temperature-programmed reduction / oxidation (H_2-TPR / O_2-TPO), scanning electron microscopy (SEM) and energy dispersive X-ray spectroscopy (EDS) before and after cyclic thermogravimetric analysis (TGA, section 2.3).

Powder diffraction data was collected using a Bruker D8 Advance Diffractometer (Cu K_α, λ = 1.5460 Å, 40.0 kV / 40.0 mA) with a Göbbel mirror and a spinning flat plate or capillary configuration. A Rietveld refinement (Rietveld, 1969) was performed using TOPAS software (using an 8^{th} order Chebyshev polynomial background function and Thompson-Cox-Hastings pseudo-Voigt Bragg peak description (Thompson et al., 1987)). Rietveld refinement guidelines from the *International Union of Crystallography - Commission on Powder Diffraction* (McCusker et al., 1999) have been followed as well as recommended practice for Rietveld refinement data presentation (Toby, 2006). Thus, the calculated weighted profile R-factor (R_{wp}) and goodness-of-fit (GoF = R_{wp}/R_{exp}, where R_{exp} is the expected R-factor (Toby, 2006)) are reported along with diffraction data, the Rietveld refinement profile and a difference curve.

Temperature-programmed desorption (TPD), reduction (H_2-TPR, hereinafter referred to as "TPR") and oxidation (O_2-TPO, hereinafter referred to as "TPO") were performed using a Micromeritics 3Flex TCD. 300.0 mg sample was used for TPD, TPR and TPO with a 10°C min^{-1} heating rate and a 50°C min^{-1} cooling rate for all tests. For TPD, the sample was heated in 50 cm^3 STP min^{-1} helium (He) at ambient pressure from ambient temperature to a 35 min 700°C dwell. TPR was performed in 50 cm^3 min^{-1} 10 vol% H_2 (balance N_2) at ambient pressure form ambient temperature to 900°C, and TPO was performed in 50 cm^3 STP min^{-1} 5 vol% O_2 (balance He) to 700°C, both utilizing a 30 min high-temperature

dwell time. In this work, temperature programmed methods have been used for studying the reduction of mixed calcium-copper phases ($CaCu_2O_3$ and Ca_2CuO_3).

A Thermo Fisher Zeiss Supra was used in the collection of scanning electron microscopy (SEM) and energy dispersive X-ray spectroscopy (EDS) data at 10.0 – 15.0 mA and 15.0 keV using a detector distance of 8.0 – 15.0 mm.

2.3 Cyclic Thermogravimetric Analysis (TGA)

The cyclic TGA testing and the TGA equipment have been reported in detail by our research group in a previous article (Westbye et al., 2018). The implemented testing regime (Table 1) simulates representative Ca-Cu Looping conditions. All materials have been tested for 45 – 50 cycles where each cycle has a 159 min duration (50 cycles equals 5.5 days of continuous testing). Synthetic air (21 vol% O_2, 79 vol% N_2, 6.0, Praxair), CO_2 (5.0, Praxair), steam (H_2O(g), deionized), H_2 (6.0, Praxair) and N_2 (5.0, Praxair) are available to the experimental set-up. The TGA is operated with a 500 mL STP min^{-1} total flow and 9.0°C min^{-1} and 3.5°C min^{-1} heating and cooling rates, respectively. Carbonation is performed at 650°C with steam in 15 vol% CO_2, and oxidation is performed at 650°C using 5.3 vol% O_2. CO_2 is introduced in the oxidation step to limit calcination during oxidation. Reduction and calcination are performed in a carbonaceous environment (40 vol% CO_2) at 870°C using hydrogen.

Table 1. Conditions for cyclic TGA testing. The total flow is 500 mL STP min^{-1} with heating and cooling rates of 9.0°C min^{-1} and 3.5°C min^{-1}, respectively.

	Time [min]	***T* [°C]**	**CO_2 [vol%]**	**N_2 [vol%]**	**H_2O [vol%]**	**H_2 [vol%]**	**Air [vol%]**
1. Carbonation	35	650	15	60	25	0	0
2. Oxidation	25	650	75	0	0	0	25
3. Heating	25	650 to 870	80	0	10	0	10
4. Calcination	8	870	40	35	25	0	0
5. Reduction	3	870	40	15	25	20	0
6. Cooling	63	870 to 650	0	70	25	5	0

In a TGA test, 25 mg sample is heated in a calibrated alumina crucible in 400 mL STP min^{-1} synthetic air and 100 mL STP min^{-1} N_2 to 870°C, flushed for 3 min in pure N_2 and subjected to the described calcination, reduction and cooling steps (Table 1, steps 4 – 6). The material is thus calcined and reduced before the cyclic testing is initiated. After the 50^{th} cooling step the test is stopped, and the material is cooled to room temperature in 500 mL STP min^{-1} synthetic air. All materials where in a calcined and oxidized state during characterization. CO_2 and O_2 carrying capacities are reported on a 100.0 g $CaO/Cu/CaZrO_3$ basis as gCO_2/100g and gO_2/100g. Compositional estimates are given on a $CaO/CuO/CaZrO_3$ basis in wt%.

The expected theoretical TGA capacity for the three synthesized materials are 17.1 gCO_2/100g and 8.7 gO_2/100g for CuO40_R2 (20/40/40 wt% $CaO/CuO/CaZrO_3$), 21.8 gCO_2/100g and 11.2 gO_2/100g for CuO50_R2 (25/50/25 wt% $CaO/CuO/CaZrO_3$) and 3.4 gCO_2/100g and 8.7 gO_2/100g for CuO40_R10 (4/40/56 wt% $CaO/CuO/CaZrO_3$).

3. Results and Discussion

3.1 Combined Calcium Zirconate Materials with a CuO/CaO Ratio of 2 [wt/wt]

3.1.1 Materials Characterization Prior to TGA Testing

Powder X-ray Diffraction Data (PXRD)

All Bragg peaks have been accounted for and identified as CaO, CuO, $CaZrO_3$, $CaCu_2O_3$ and Ca_2CuO_3 in the X-ray diffraction data collected for CuO40_R2 and CuO50_R2 (Figure 1). Mixed calcium-copper phases were expected as they have been observed in combined materials based on mayenite (CaO/CuO/$Ca_{12}Al_{14}O_{33}$) (Westbye et al., 2018). For mayenite materials, these mixed phases segregated into separate CaO and CuO phases during cyclic TGA testing. Mixed phases are more thoroughly investigated using temperature-programmed methods (Figure 4). The Rietveld refinements, backgrounds and difference curves are deemed acceptable (Figure 1). Reported R_{wp} values and GoF (Table 2) are within a reasonable range for Rietveld refinement. No sodium (Na) compounds were identified though amorphous species cannot be excluded. Non-crystalline species are, if at all present, only expected in trace amounts and are considered insignificant for the presented results.

By comparing the diffraction patterns of CuO40_R2 and CuO50_R2 (Figure 1) it is evident that the same Bragg peaks are found in both samples though the relative peak intensities are different. In the pattern for CuO40_R2, peaks related to $CaZrO_3$ are more intense relative to those of mixed calcium-copper phases and CuO. The opposite is true for CuO50_R2. These observations are in line with the theoretical compositions of the synthesized materials, as CuO50_R2 has the highest calcium and copper loading while CuO40_R2 has a higher Zr content.

Qualitative observations from the graph of PXRD patterns are reflected in Rietveld refinement data (Table 2). The CuO50_R2 material has a higher weight fraction of CuO and a lower mass content of $CaZrO_3$ relative to CuO40_R2. Calcium is predominantly present in the mixed phases Ca_2CuO_3 and $CaCu_2O_3$ in both samples. Zirconium is solely found in the $CaZrO_3$ phase, an indication that the selected calcination conditions (950°C, 1 h) are appropriate for $CaZrO_3$ formation. Expected material compositions in calcined and oxidized states calculated from Rietveld refinement data, assuming that all Ca and Cu present as CuO, CaO, $CaCu_2O_3$ and Ca_2CuO_3 will be available for sorption, are as follows: 16.6/42.8/40.6 wt% CaO/CuO/$CaZrO_3$ for CuO40_R2 with 14.3 gCO_2/100g and 9.4 gO_2/100g expected sorption capacities and 24.9/55.2/19.9 wt% CaO/CuO/$CaZrO_3$ for CuO50_R2 with 21.2 gCO_2/100g and 12.7 gO_2/100g expected carrying capacities. This is in good agreement with the compositions expected from the syntheses.

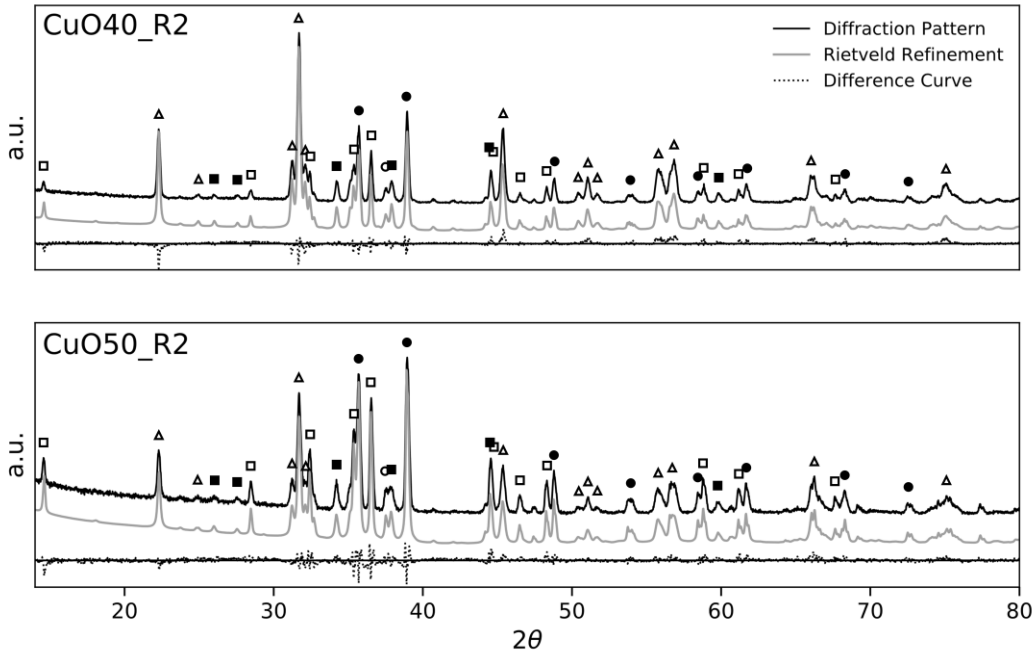

Figure 1. Diffraction patterns (black), Rietveld refinement profiles (grey) and difference curves (black, dotted) for calcined CuO/CaO = 2.0 [wt/wt] powders before TGA testing. Data was collected using a spinning flat plate configuration. Identified phases: CaO (○), CuO (●), $CaZrO_3$ (Δ), $CaCu_2O_3$ (■) and Ca_2CuO_3 (□).

Table 2. Quantitative data from Rietveld refinement for CuO/CaO = 2.0 [wt/wt] materials prior to TGA testing. Data are given on a weight percent (wt%) basis, R_{wp} [%] is the weighted R-factor and GoF [-] is the profile goodness-of-fit.

	CuO [wt%]	**CaO [wt%]**	**$CaZrO_3$ [wt%]**	**$CaCu_2O_3$ [wt%]**	**Ca_2CuO_3 [wt%]**	**R_{wp} / GoF**
CuO40_R2	23.9	1.5	40.6	15.1	18.9	12.85 / 2.13
CuO50_R2	31.8	2.7	19.9	13.9	31.7	10.71 / 1.79

Scanning Electron Microscopy (SEM) and Energy Dispersive X-ray Spectroscopy (EDS)

The elemental dispersion of Ca, Cu and Zr in CuO40_R2 (Figure 2) and CuO50_R2 (Figure 3) before TGA testing is rather homogeneous. The Cu distribution in CuO50_R2 is slightly more clustered relative to that of CuO40_R2. This could be expected due to the higher CuO content of CuO50_R2 (Table 2). In the CaO/$CaZrO_3$ sorbent prepared by Zhao et al. (Zhao et al., 2014), cuboids of $CaZrO_3$ were observed in SEM / TEM. These cuboids have not been observed in the combined material powders in this work. This can indicate that the implemented procedure, using Na_2CO_3 while introducing copper, either hinders or severely limits $CaZrO_3$ cuboid formation.

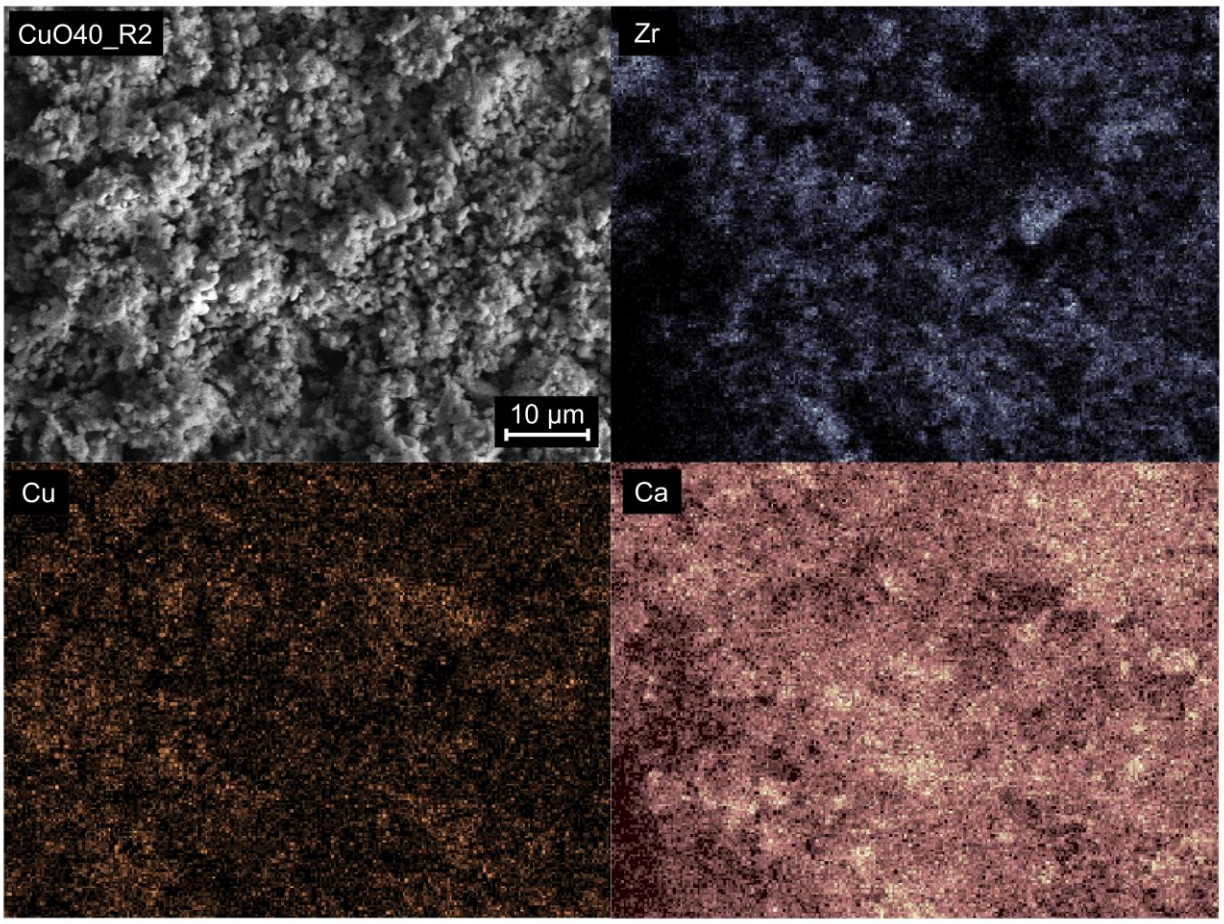

Figure 2. A surface SEM image and elemental EDS mapping (Zr, Cu and Ca) for CuO40_R2 (15.0 keV, 8.5 mm detector distance, 5.00 KX magnification).

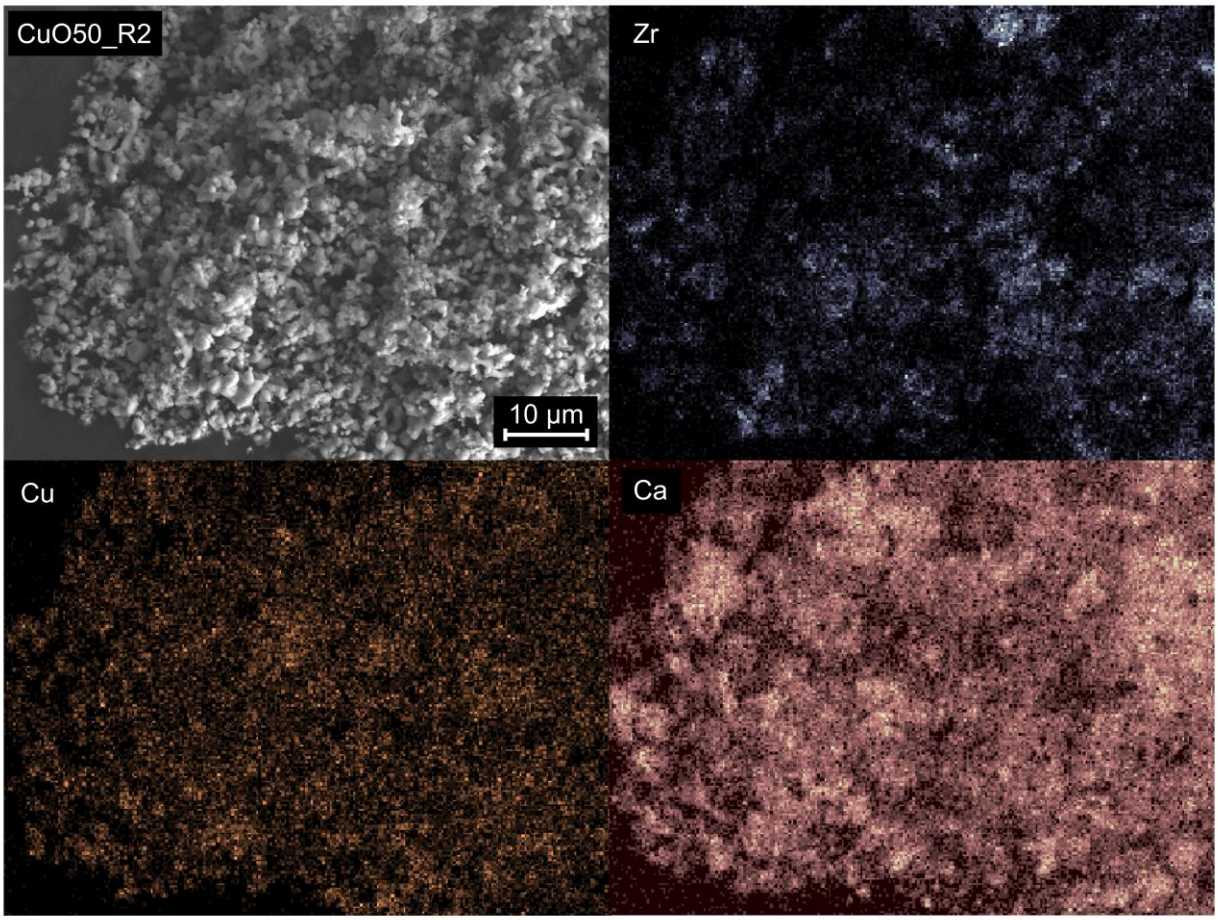

Figure 3. A surface SEM image and elemental EDS mapping (Zr, Cu and Ca) for CuO50_R2 (15.0 keV, 8.5 mm detector distance, 5.00 KX magnification).

Temperature-Programmed Reduction and Oxidation of CuO40_R2

There is limited data on mixed calcium-copper phase reactivity reported in literature, though some physical data has been reported (Fouad et al., 2012) (Hess et al., 2007). In order to further investigate the $CaCu_2O_3$ and Ca_2CuO_3 mixed phases observed in the combined material, and to ensure that an 870°C reduction temperature is indeed sufficient for the complete reduction of mixed phases, the CuO40_R2 material was subjected to three consecutive TPR / TPO measurements. A TPD was performed prior to these measurements in order to remove volatile contaminants (e.g. H_2O from potential traces of $Ca(OH)_2$) that could interfere with TPR / TPO data interpretation. A PXRD pattern was recorded after the third TPO for examination of the phase composition. TPR results are given along with a CuO powder H_2-TPR reference pattern superimposed on the data (Figure 4). TPO results and the PXRD pattern are provided in the Supporting Information (Figure S1 and Figure S2, respectively).

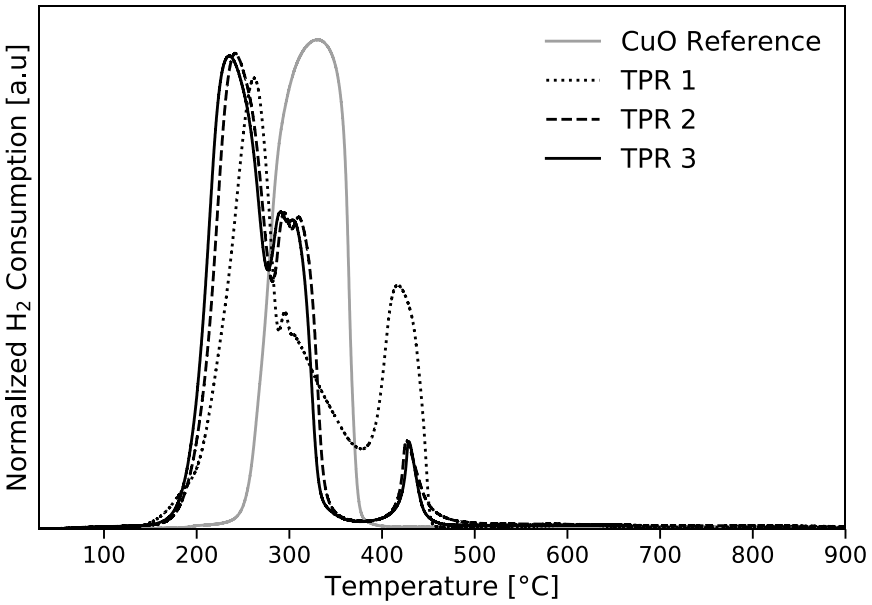

Figure 4. Results for three TPR experiments with initial TPD and intermediate TPO. TPR was performed using a 50 cm^3 STP min^{-1} 10 / 90 vol% H_2 / N_2 flow, a 10°C min^{-1} heating rate from ambient conditions to 900°C and a 50°C min^{-1} cooling rate. Approximately 130 cm^3 STP H_2 g^{-1} was consumed in all three TPR experiments. Peak positions from left to right: TPR 1 (268°C, 300°C, 418°C), TPR 2 (242°C, 294°C, 309°C, 427°C), TPR 3 (235°C, 290°C, 304°C, 429°C) and CuO reference (331°C)

It is evident from TPR data (Figure 4) that the sample is completely reduced at 418 - 429°C for all three TPR runs. The hydrogen consumption was approximately 130 cm^3 STP H_2 g^{-1} in each test, in good agreement with the expected copper content (the oxygen consumption during TPO tests was ca. 73 cm^3 STP O_2 g^{-1}, in agreement with the H_2 consumption). The PXRD data after the third TPO (Supporting Information, Figure S2) revealed that only CuO, CaO and $CaZrO_3$ phases were present in the sample. This implies that mixed calcium-copper phases can be expected to completely reduce at high temperature (> 430°C) and that only separate CaO and CuO phases are formed upon subsequent oxidation. The presence of mixed phases in the synthesized material is therefore not expected to affect the cyclic performance of the material as all processing steps during TGA testing (and Ca-Cu Looping) are above 430°C. TPO data (Supporting Information, Figure S1) along with the measured O_2 consumption suggests the sample is completely oxidized at 650°C.

The discrepancies between TPR 1 and TPR 2 / TPR 3 patterns have been attributed to the presence of mixed phases in TPR 1 and their absence during TPR 2 and TPR 3. The peak positions for TPR 2 and TPR 3 are (from left to right, TPR 2 / TPR 3): 242°C / 235°C, 294°C / 290°C, 309°C / 304°C and 427°C / 429°C. The difference between TPR 2 and TPR 3 profiles is a slight shift towards lower temperatures in TPR 3 relative to TPR 2. This indicates that the sample is more easily reduced after exposure to consecutive TPR / TPO runs. The general shapes of the TPR 2 / TPR 3 patterns in the approximate range 235 – 305°C correspond well with other TPR patterns for supported copper materials reported in literature (Cabello et al., 2016) (Zhou et al., 1999). Of special note is the reported peak at 241.2°C for a mixed CuO-Cu_2O-Cu phase by Y. Zhai et al. (Zhai et al., 2015), similar to the TPR 2 / TPR 3 peaks located at 242°C / 235°C. The peaks located around 300°C could also be attributed to CuO reduction, as the profile overlap between the reference H_2-TPR CuO powder match well with the TPR 2 / TPR 3 profile shape. The reference H_2-TPR CuO pattern is in line with that reported for CuO in literature (L. Díez-Martín et al., 2018a) (Laura Díez-Martín et al., 2018). It is of note that a significant portion of copper present in the combined material is seemingly more easily reduced than the CuO reference

powder. The exact reasons for the ease of reduction of the prepared material relative to pure CuO requires further dedicated investigation and is out of the scope of this paper (e.g. in situ XRD studies). However, there have been reports that Zr doping can improve CuO reactivity (Wang et al., 2015) and the particle size and presence of mixed oxides during reduction could affect the reducibility of copper.

The last TPR peak located at 418 – 429°C for all TPR tests has been attributed to mixed calcium-copper phases as the total peak area decreases significantly from TPR 1 to TPR 2 / TPR 3. The 418°C peak area is a substantial fraction of the TPR 1 pattern, but it is only responsible for 3.9 – 4.0 cm^3 STP H_2 g^{-1} consumption out of 130 cm^3 STP H_2 g^{-1} for TPR 2 and TPR 3. In order to support this claim, a fourth TPR was performed using the same experimental conditions but halting the reduction at 340°C and cooling the sample in pure N_2 to avoid further reduction (*not shown*). In the PXRD pattern of this TPR 4, Cu, CaO and $CaZrO_3$ peaks were found, with minute contributions from mixed phases. Given that no mixed phases were found in the oxidized sample following complete reduction and the H_2 consumption for all TPR runs were the same with the 420 – 430°C TPR peak found in all samples, it could be possible that mixed phases form in small amounts during the 235 – 305°C range reduction, and that these formed mixed phases are not completely reduced until a temperature of 418 – 429°C is reached. This interaction is however not deemed particularly significant as (1) there are only trace amounts of mixed phase being formed (2) the Ca-Cu Looping reduction is performed at 870°C, and (3) in the Ca-Cu Looping process Ca will be present as $CaCO_3$ during oxidation and partially so during reduction, thus the potential for CaO-CuO interaction is more limited.

3.1.2 Evaluation of Material Performance in Cyclic TGA Testing

Cyclic TGA results for CuO40_R2 and CuO50_R2 are given in Figure 5. The CO_2 and O_2 carrying capacities for CuO40_R2 were stable at 13.6 gCO_2/100g and 8.2 – 8.6 gO_2/100g throughout cycling, resulting in an observed active composition of 16.0/39.6/44.4 wt% CaO/CuO/$CaZrO_3$ (Table 3) at full oxidation and carbonation (i.e. including kinetic- and diffusion-controlled CaO carbonation). This compositional estimate from cyclic TGA is in good agreement with that expected from Rietveld refinement (16.6/42.8/40.6 wt%) and synthesis stoichiometry (20/40/40 wt%), implying that most of the Cu and free CaO in the sample are involved in gas sorption.

The carbonation and oxidation profiles of CuO40_R2 (Figure 6 (a)) have a slight increase in total sorption capacity from cycle 5 to 25. Profile shapes and carrying capacities are unaltered from the 25th cycle and throughout the remaining 50 cycles. The observed CaO carbonation is typical for CaO based sorbents, characterized by an initial linear weight increase (kinetic regime) followed by a progressively diminishing rate of carbonation (diffusion regime) resulting in a curved weight change profile. Copper oxidation in CuO40_R2 is dominated by a kinetic regime even at a low 5.3 vol% O_2 fraction in the gas phase at 650°C. This oxidation behaviour occurs in spite of $CaCO_3$ being present in the combined material which could potentially reduce the powder sample porosity. A significant observation is that both CO_2 and O_2 carrying capacities are stable from the first cycle. Stable and predictable active CuO and CaO loadings in synthesized combined materials are of great importance as they affect the Ca-Cu Looping energetics through the CuO/CaO ratio. Combined materials must be synthesized using a pre-determined CuO/CaO ratio, implying that stable and predictable capacities are vital for tailoring these materials towards various Ca-Cu Looping process configurations and/or feedstocks.

CuO50_R2 is losing O_2 carrying capacity throughout cycling (Figure 5). Inspecting the carbonation and oxidation curves of CuO50_R2 (Figure 6 (b)), it is clear that the O_2 capacity is decreasing already from cycle 5, while the CO_2 capacity is slightly increasing until the 25th cycle and deactivates as the oxygen carrying function decays further. This initial slight increase in CO_2 sorption

could be caused by physical changes in the powder or possibly due to a slight increase in active CaO content caused by gradual disappearance of mixed Ca-Cu phases during the first cycles (traces of mixed phases were detected in CuO50_R2 after 10 TGA cycles, section 3.1.3, Figure 7). It was shown in section 3.1.1 that mixed calcium-copper phases are expected to completely reduce, however, this is only valid if all material is completely exposed to the reducing gas. The higher copper loading and mixed phase content in the CuO50_R2 sample could to some extent hinder gas diffusion, resulting in a more gradual disappearance of mixed phases. In any case, the eventual decline in both CO_2 and O_2 carrying capacities can be attributed to severe copper migration and agglomeration (section 3.1.3).The general curve shapes for carbonation and oxidation are similar for CuO50_R2 and CuO40_R2 (Figure 6). The compositional estimate for CuO50_R2 from TGA testing based on maximum carrying capacities of 22.0 gCO_2/100g and 11.3 gO2/100g is 25.1/50.6/23.3 wt% CaO/CuO/$CaZrO_3$ (Table 3). This compares well with the Rietveld refinement estimate of the composition of the calcined and oxidized material (24.9/55.2/19.9 wt%) and that expected from synthesis stoichiometry (25/50/25 wt%).

Other combined materials reported in literature have displayed the opposite trend to that presented here with sorbent deactivation and copper stability being more commonly observed (Manovic and Anthony, 2011) (Manovic et al., 2011) (Kierzkowska and Müller, 2012) (Kierzkowska and Müller, 2013). The reason for this observation is not clear at this point, though the rather harsh testing conditions used in this work and the use of steam during carbonation and calcination / reduction can play significant roles. In general, and as mentioned in the introduction, it is not straight forward to directly compare the presented combined material and other combined materials due to the varying testing conditions employed. However, it is interesting to note that the described behaviour of the CaO/CuO/$CaZrO_3$ 40 and 50 wt% CuO loaded materials CuO40_R2 and CuO50_R2 are similar to those obtained for mayenite based materials (CaO/CuO/$Ca_{12}Al_{14}O_{33}$) at a CuO/CaO = 2.0 [wt/wt] observed in our previous work (Westbye et al., 2018), where 50 wt% CuO loaded materials deactivated regardless of CuO precursor (CuO powder, $Cu(OH)_2$ and $Cu(NO_3)_2$) while 40 wt% loaded materials remained stable throughout cycling.

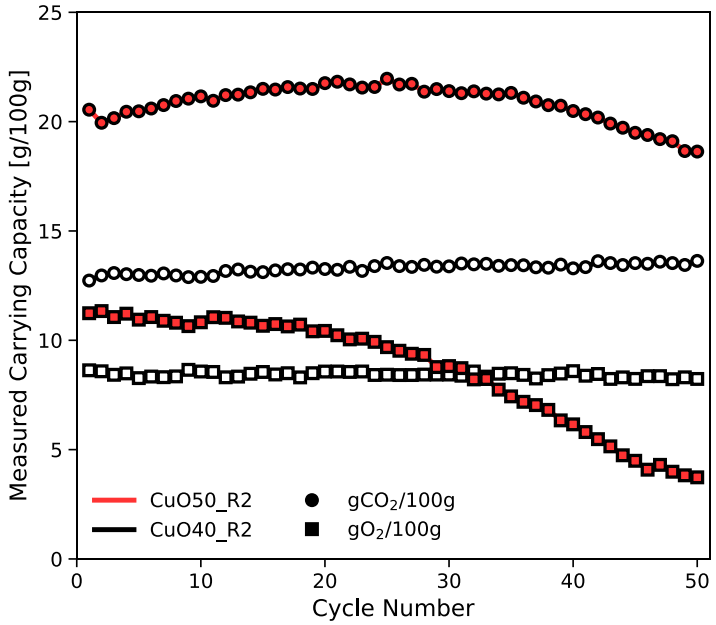

Figure 5. Sorption capacities during cyclic TGA testing of CuO50_R2 and CuO40_R2. Capacities are given in gram per 100.0 gram (g/100g) calcined and reduced material (CaO/Cu/$CaZrO_3$). Testing conditions are given in Table 1.

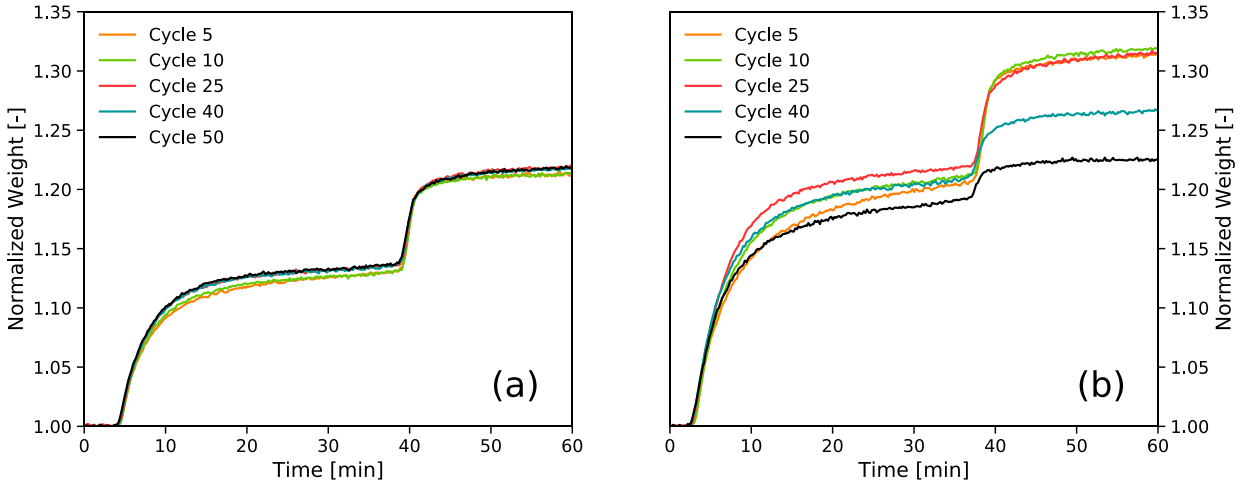

Figure 6. Carbonation (5 min mark) and oxidation (40 min mark) profiles for materials during cyclic TGA testing. (a) CuO40_R2. (b) CuO50_R2. Sample weight is normalized using the reduced and calcined ($CaO/Cu/CaZrO_3$) weight before cycle initiation for each cycle.

Table 3. Results from cyclic TGA testing for CuO40_R2 and CuO50_R2 powders. Subscript "*max*": highest recorded carrying capacity. Subscript "*50*": Carrying capacity in the 50th cycle. Carrying capacities are given per 100.0 grams of reduced and calcined material ($CaO/Cu/CaZrO_3$).

	CuO40_R2	**CuO50_R2**
$[gCO_2/100g]_{max}$	13.6	22.0
$[gO_2/100g]_{max}$	8.6	11.3
$(CaO/CuO/CaZrO_3)_{max}$ wt%	16.0/39.6/44.4	25.1/50.6/23.3
$[gCO_2/100g]_{50}$	13.6	3.7
$[gO_2/100g]_{50}$	8.2	18.6
$(CaO/CuO/CaZrO_3)_{50}$ wt%	16.0/37.8/46.2	22.2/17.7/60.1

3.1.3 Materials Characterization After Cyclic TGA Testing

Powder X-ray Diffraction Data (PXRD)

During a preliminary screening of combined materials, 10 TGA cycles were performed on samples from the CuO40_R2 and CuO50_R2 batches prior to 50 TGA cycles (Figure 7). In line with what was observed in PXRD data prior to TGA testing (Figure 1), the relative intensities of $CaZrO_3$, CaO and CuO are different for CuO40_R2_T10 and CuO50_R2_T10, where $CaZrO_3$ is more pronounced in the former and CuO and CaO are more pronounced in the latter. No mixed phases were observed in the PXRD diffraction data (Figure 7) for CuO40_R2_T10 - the mixed phases had segregated into separate CaO and CuO phases as expected from TPR data (Figure 4, section 3.1.1). Trace amounts of $CaCu_2O_3$ were observed for CuO50_R2_T10 (Figure 7). Gradual disappearance of mixed calcium-copper phases can be an explanation for the slight increase in CO_2 capacity for CuO50_R2 (Figure 5, section 3.1.2) during the first 25 cycles. A PXRD was performed (*not shown*) on the CuO50_R2_T50 to check for mixed phases. No mixed phases were present, indicating that the mixed phases had completely segregated after 50 TGA cycles.

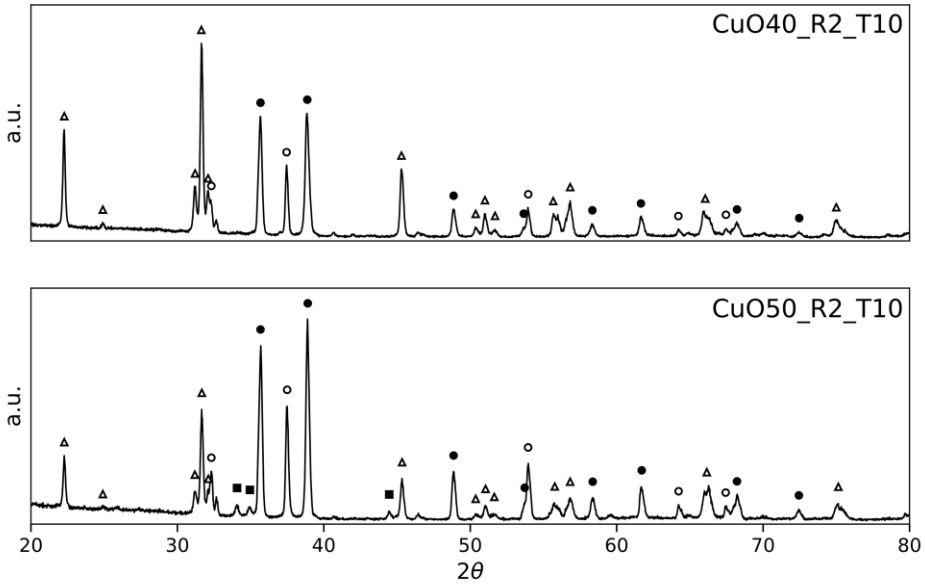

Figure 7. Diffraction patterns of CuO/CaO = 2.0 [wt/wt] powders after 10 TGA cycles. Data was collected using a spinning flat plate configuration. Identified phases: CaO (○), CuO (●), $CaZrO_3$ (∆) and $CaCu_2O_3$ (■).

Scanning Electron Microscopy (SEM) and Energy Dispersive X-ray Spectroscopy (EDS)

From the SEM images and EDS analysis for the samples after 10 and after 50 TGA cycles (Figure 8 and Figure 9) it seems evident that there has been copper migration and agglomeration in both materials. The agglomeration is severe for CuO50_R2_T50. Copper migration can explain the significant loss of CO_2 and O_2 carrying capacities for CuO50_R2 during cycling (Figure 5). For both materials the segregation of well dispersed mixed phases (Figure 2 and Figure 3) is evident after 10 cycles where both CuO40_R2_T10 and CuO50_R2_T10 are similar with respect to the elemental distributions of Ca, Cu and Zr. However, while CuO40_R2_T10 and CuO_R2_T10 have comparable copper distributions, there is clear copper sheet formation in CuO50_R2_T50 not present in CuO40_R2_T50.

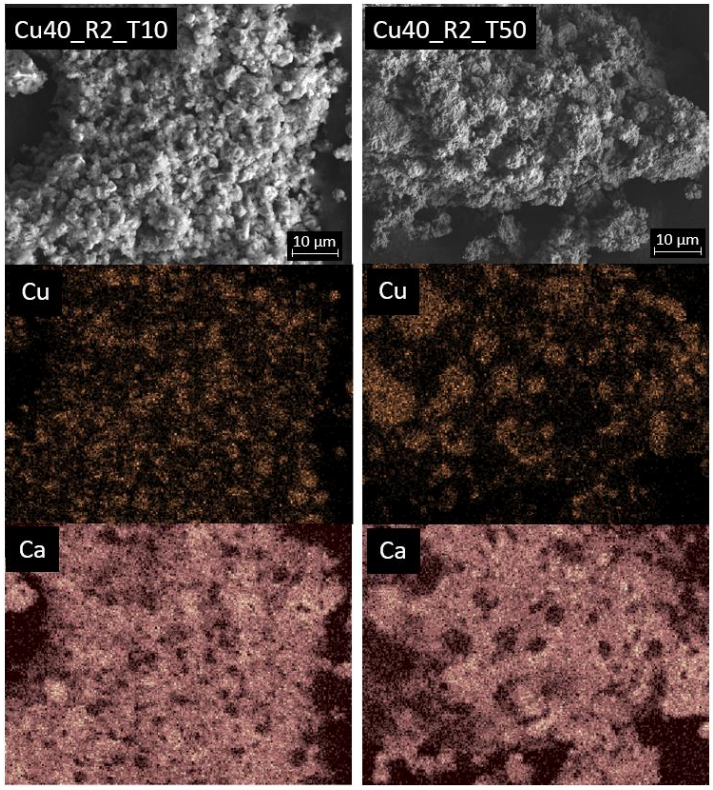

Figure 8. Surface SEM and elemental EDS mapping (Zr, Cu and Ca) for CuO40_R2 (15.0 keV, 8.5 mm detector distance, 5.00 KX magnification) after 10 (*left column*) and 50 (*right column*) TGA cycles.

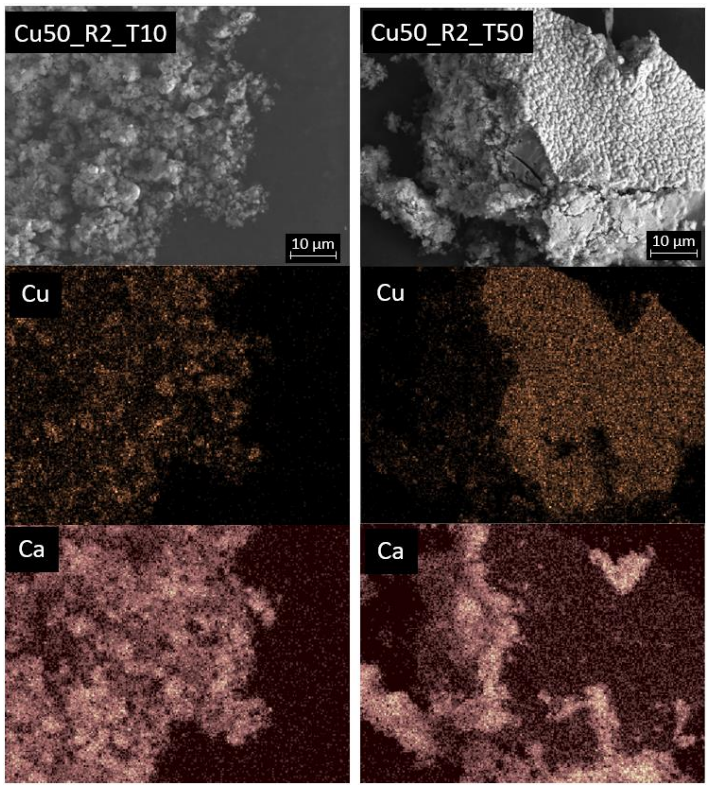

Figure 9. Surface SEM and elemental EDS mapping (Zr, Cu and Ca) for CuO50_R2 (15.0 keV, 8.5 mm detector distance, 5.00 KX magnification) after 10 (*left column*) and 50 (*right column*) TGA cycles.

3.2 A Combined Calcium Zirconate Material with a CuO/CaO Ratio of 10 [wt/wt]

Combined material candidates for Ca-Cu Looping must display stable CO_2 and O_2 capture capacities at various CuO/CaO ratios due to the different energetic requirements for various Ca-Cu Looping configurations and reducing gas compositions. In order to investigate the effect of CuO/CaO ratio on the stable CuO40_R2 material presented in section 3.1, a CuO40_R10 material was synthesized. The copper loading was the same as in CuO40_R2, though the active CaO content was lowered and substituted for the high-Tammann temperature $CaZrO_3$ phase. CuO40_R10 has been subjected to the same characterization and TGA testing presented in section 3.1. The expected active composition of CuO40_R10 is 4/40/56 wt% CaO/CuO/$CaZrO_3$ from stoichiometric considerations.

A PXRD pattern of CuO40_R10 prior to TGA testing (Figure 10) identified CaO, CuO, $CaZrO_3$ and $CaCu_2O_3$ phases. The absence of Ca_2CuO_3 is likely due to the low CaO content. A Rietveld refinement was performed for this material giving an estimated composition of 3.5/41.6/54.9 wt% CaO/CuO/$CaZrO_3$ (R_{wp}/GoF of 54.9/11.3). This PXRD result was obtained using a capillary configuration in contrast to the spinning flat plate configuration used for all CuO40_R2 and CuO50_R2 samples. This is believed to be the cause of the relatively high R_{wp}/GoF values. Though the R_{wp}/GoF values for the capillary PXRD Rietveld refinement data could be considered too high for accurate compositional estimates, the result corresponds well with the composition expected from synthesis stoichiometry (4/40/56 wt% CaO/CuO/$CaZrO_3$) and the active composition obtained from TGA (Figure 11). The PXRD pattern along with the Rietveld refinement and a difference curve is presented in the Supporting Information (Figure S3).

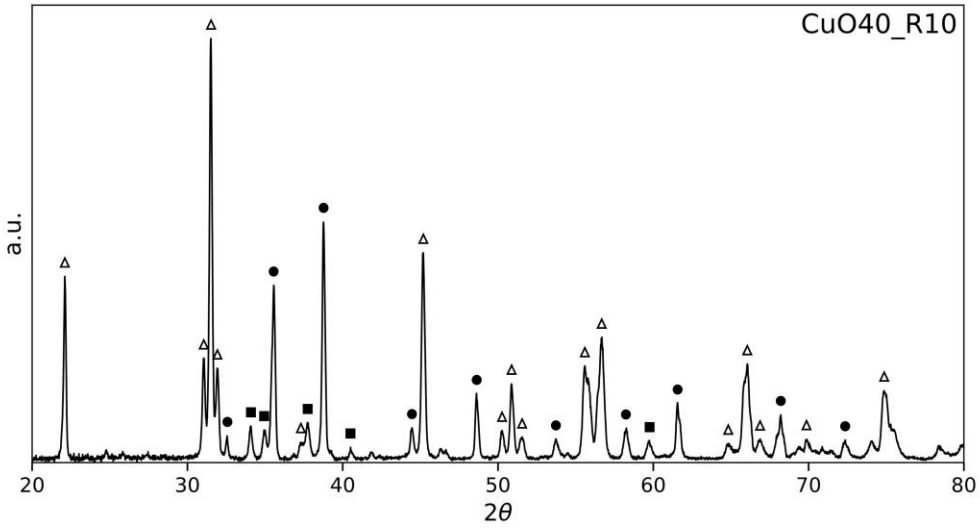

Figure 10. Diffraction pattern of CuO40_R10 powder prior to cyclic TGA. Data was collected using a capillary configuration. Identified phases: CaO (○), CuO (●), $CaZrO_3$ (Δ) and $CaCu_2O_3$ (■).

CuO40_R10 was exposed to 45 TGA cycles (Figure 11). Stable carrying capacities of 3.5 gCO_2/100g and 9.6 gO_2/100g were recorded from the first cycle and throughout cycling. This is equivalent to a 4.1/43.5/52.4 wt% CuO/CaO/$CaZrO_3$ composition (CuO/CaO = 10.6 [wt/wt]). The carbonation curve is as expected at a lower level compared to the CuO/CaO = 2.0 [wt/wt] materials (Figure 6) and seems to

be quite diffusion dominated. Both observations can be attributed to the low CaO loading. Copper oxidation curves are similar for CuO40_R2 and CuO40_R10.

The cyclic stabilities of CuO40_R2 and CuO40_R10 are an indication that 40 wt% CuO loaded combined materials do in fact have a tuneable CuO/CaO ratio in a Ca-Cu Looping relevant range of ≥ 2.0 [wt/wt] (conclusions cannot be drawn about decreasing the CuO/CaO ratio below 2.0). The cyclic stability does not seem to be negatively affected by reducing the active CaO content and replacing it with $CaZrO_3$ for CuO/CaO ratio tuning.

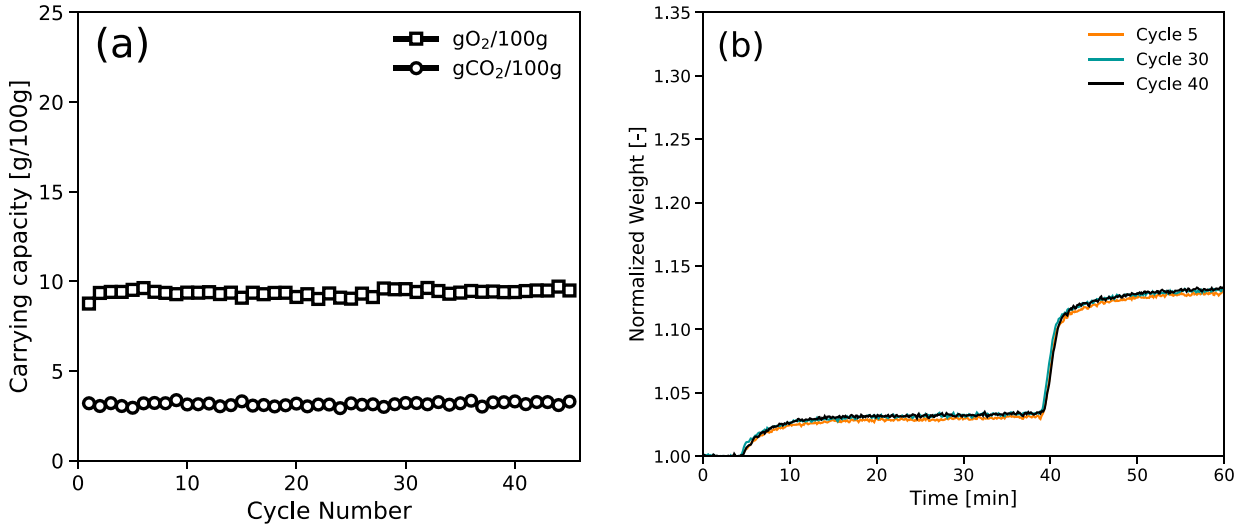

Figure 11. (a) Sorption capacities and (b) carbonation (5 min mark) and oxidation (40 min mark) profiles during cyclic TGA testing of CuO40_R10. Testing conditions are given in Table 1. Sorption capacities are given in gram per 100.0 gram (g/100g) calcined and reduced material ($CaO/Cu/CaZrO_3$). The sample weight in (b) is normalized using the reduced and calcined weight before cycle initiation for each cycle.

From the SEM/EDS data (Figure 12) of CuO40_R10, which compares fresh material and CuO40_R10_T45, it seems that the lack of mixed phases results in a slightly poorer elemental dispersion of Ca, Cu and Zr in CuO40_R10 relative to CuO40_R2 (Figure 2) with spherical copper clusters already present in the fresh CuO40_R10 sample. The copper spheres observed in the fresh material are given in Figure 13, where it is seen that the spherical copper particles (1 – 2 μm in diameter) are embedded in a matrix-like $CaO/CaZrO_3$ structure. It is of note that CuO40_R10 before TGA cycling look similar to CuO40_R2_T10 and CuO50_R2_T10 after the mixed phases have mostly segregated into CaO and CuO phases. In CuO40_R10_T45 (Figure 12) there has been copper migration and agglomeration as observed for CuO40_R2_T50 and CuO50_R2_T50, though the copper clusters are still spherical and well dispersed throughout the material.

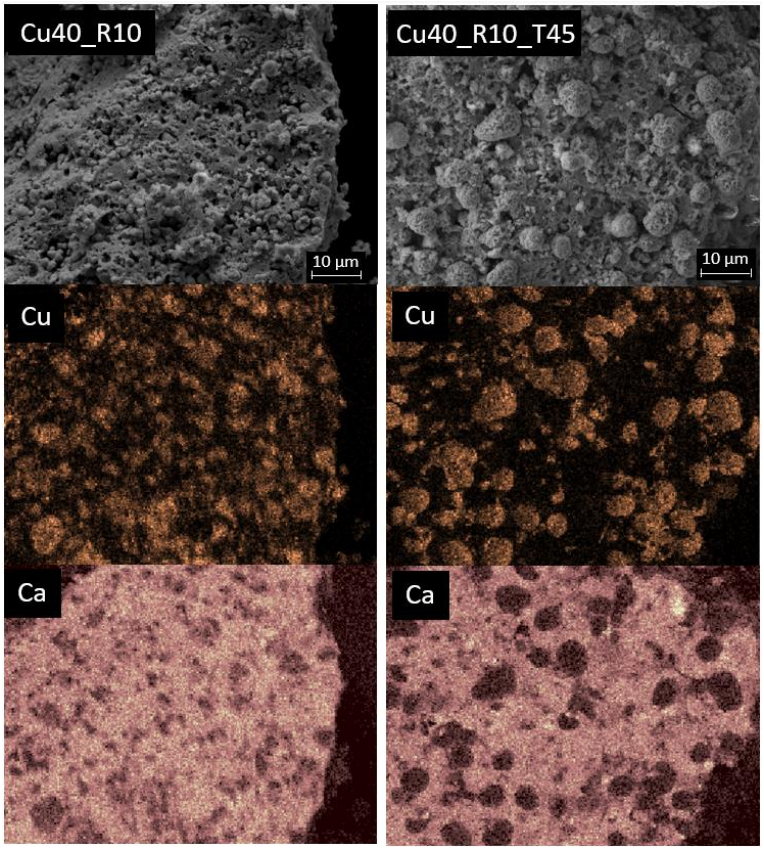

Figure 12. Surface SEM and elemental EDS mapping (Zr, Cu and Ca) for CuO40_R10 fresh and after 45 TGA cycles (15.0 keV, 8.5 mm detector distance, 5.00 KX magnification) fresh and after 45 TGA cycles.

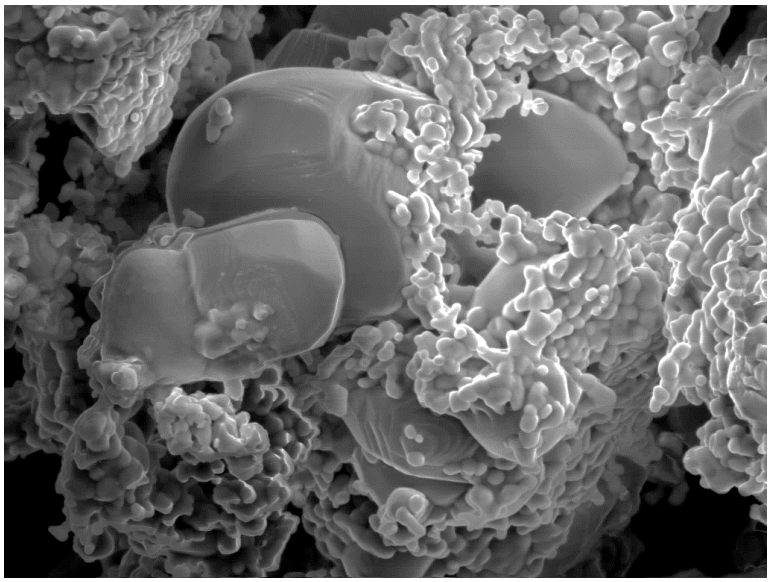

Figure 13. A SEM surface image of CuO40_R10 taken with an InLens lens at 40.00 KX resolution and 3.5 mm detector distance at 5.00 keV. The diameter of the copper spheres is 1 – 2 µm.

4. Conclusions

Combined calcium-copper materials based on calcium zirconate, $CaO/CuO/CaZrO_3$, for Ca-Cu Looping have been synthesized, characterized and tested under 45 - 50 process relevant TGA cycles. A material prepared using a CuO/CaO = 2.0 [wt/wt] and 50 wt% active CuO loading was shown to deactivate during cycling due to copper migration and agglomeration, while 40 wt% CuO loaded combined materials at CuO/CaO mass ratios of 2 and 10 were stable throughout TGA testing. This indicates that 40 wt% active CuO loaded materials based on $CaZrO_3$ are suitable candidates for further development for Ca-Cu Looping. Given the stable behaviour at CuO/CaO mass ratios of 2 and 10, it is highly likely that the material is stable for CuO/CaO ratios in the range [2,10], assuming that the copper loading is kept constant and the ratio is tuned by changing the CaO mass content. O_2 and CO_2 g/100g capacities were stable from the first cycle for CuO40_R2 and CuO40_R10, a significant finding considering the importance of predictable CuO/CaO ratios for tuning materials towards various Ca-Cu Looping processing configurations.

Mixed calcium-copper phases $CaCu_2O_3$ and Ca_2CuO_3 were observed in PXRD patterns and are not believed to interfere with Ca-Cu Looping performance: Temperature-programmed methods were used to demonstrate that the material is completely reduced at 430°C and that complete oxidation can be expected at 650°C. Rietveld refinement of PXRD patterns gave good predictions of expected active phase composition in agreement with TGA results and synthesis stoichiometry. SEM/EDS show that the initial dispersion of Ca, Cu and Zr is good for all prepared samples and that copper migration and agglomeration is expected to some extent in all samples after TGA testing. The slight copper migration did not seem to affect the 40 wt% loaded materials performance.

There are similarities between previously studied mayenite based combined materials ($CaO/CuO/Ca_{12}Al_{14}O_{33}$) (Westbye et al., 2018) and the presented $CaZrO_3$ materials. It is interesting to note that the optimum CuO loading for both materials likely is in the range [40, 50) wt% active CuO (CuO/CaO ≥ 2.0 [wt/wt]) - it seems the migration and agglomeration of the supported Cu species occur under the specified conditions in spite of an increase in the Tammann temperature of the supporting structure ($CaZrO_3$ versus $Ca_{12}Al_{14}O_{33}$).

The next step in $CaO/CuO/CaZrO_3$ materials development is to agglomerate the presented powder using various techniques and to assess the effect of powder agglomeration on TGA performance. The agglomerates should thereafter be tested at Ca-Cu Looping conditions in a fixed bed reactor at larger scale (e.g. ≥ 100.0 g). Development of standardized TGA tests for Ca-Cu Looping materials could also be of great value: Materials reported in literature are not directly comparable with respect to performance given the discrepancies in testing conditions and standardized testing could provide a platform for a more rigorous comparisons of candidate materials.

Acknowledgements

The presented work was funded by The Research Council of Norway (NFR) within the CLIMIT programme project "*Innovative materials for CO_2 Capture by Combined Calcium-Copper Cycles*" (project number 254736).

References

Abanades, J.C., Murillo, R., Fernandez, J.R., Grasa, G., Martínez, I., 2010. New CO2 Capture Process for Hydrogen Production Combining Ca and Cu Chemical Loops. Environ. Sci. Technol. 44, 6901–6904. https://doi.org/10.1021/es101707t

Adánez, J., de Diego, L.F., García-Labiano, F., Gayán, P., Abad, A., Palacios, J.M., 2004. Selection of Oxygen Carriers for Chemical-Looping Combustion. Energy Fuels 18, 371–377. https://doi.org/10.1021/ef0301452

Arjmand, M., Keller, M., Leion, H., Mattisson, T., Lyngfelt, A., 2012. Oxygen Release and Oxidation Rates of $MgAl_2O_4$-Supported CuO Oxygen Carrier for Chemical-Looping Combustion with Oxygen Uncoupling (CLOU). Energy Fuels 26, 6528–6539. https://doi.org/10.1021/ef3010064

Baker, E.H., 1962. 87. The calcium oxide–carbon dioxide system in the pressure range 1—300 atmospheres. J Chem Soc 0, 464–470. https://doi.org/10.1039/JR9620000464

Broda, M., Müller, C.R., 2014. Sol–gel-derived, CaO-based, ZrO2-stabilized CO2 sorbents. Fuel 127, 94–100. https://doi.org/10.1016/j.fuel.2013.08.004

Cabello, A., Gayán, P., Abad, A., de Diego, L.F., García-Labiano, F., Izquierdo, M.T., Scullard, A., Williams, G., Adánez, J., 2016. Long-lasting Cu-based oxygen carrier material for industrial scale in Chemical Looping Combustion. Int. J. Greenh. Gas Control 52, 120–129. https://doi.org/10.1016/j.ijggc.2016.06.023

Chen, C., Park, D.-W., Ahn, W.-S., 2014. CO2 capture using zeolite 13X prepared from bentonite. Appl. Surf. Sci. 292, 63–67. https://doi.org/10.1016/j.apsusc.2013.11.064

Chen, J., Duan, L., Donat, F., Müller, C.R., Anthony, E.J., Fan, M., 2018. Self-activated, nanostructured composite for improved CaL-CLC technology. Chem. Eng. J. 351, 1038–1046. https://doi.org/10.1016/j.cej.2018.06.176

Chen, J., Duan, L., Shi, T., Bian, R., Lu, Y., Donat, F., Anthony, E.J., 2019. A facile one-pot synthesis of CaO/CuO hollow microspheres featuring highly porous shells for enhanced CO_2 capture in a combined Ca–Cu looping process *via* a template-free synthesis approach. J. Mater. Chem. A 7, 21096–21105. https://doi.org/10.1039/C9TA04513A

Chuang, S., Dennis, J., Hayhurst, A., Scott, S., 2008. Development and performance of Cu-based oxygen carriers for chemical-looping combustion. Combust. Flame 154, 109–121. https://doi.org/10.1016/j.combustflame.2007.10.005

Díez-Martín, L., Grasa, G., Murillo, R., Martini, M., Gallucci, F., van Sint Annaland, M., 2018a. Determination of the oxidation kinetics of high loaded CuO-based materials under suitable conditions for the Ca/Cu H 2 production process. Fuel 219, 76–87. https://doi.org/10.1016/j.fuel.2018.01.064

Díez-Martín, Laura, Grasa, G., Murillo, R., Scullard, A., Williams, G., 2018. Development of Suitable CuO-Based Materials Supported on Al_2O_3, $MgAl_2O_4$, and ZrO_2 for Ca/Cu H_2 Production Process. Ind. Eng. Chem. Res. 57, 2890–2904. https://doi.org/10.1021/acs.iecr.7b05103

Díez-Martín, L., López, J.M., Fernández, J.R., Martínez, I., Grasa, G., Murillo, R., 2018b. Complete Ca/Cu cycle for H2 production via CH4 sorption enhanced reforming in a Lab-Scale fixed bed reactor. Chem. Eng. J. 350, 1010–1021. https://doi.org/10.1016/j.cej.2018.06.049

Donat, F., Müller, C.R., 2018. A critical assessment of the testing conditions of CaO-based CO2 sorbents. Chem. Eng. J. 336, 544–549. https://doi.org/10.1016/j.cej.2017.12.050

Fernández, J., Abanades, J., 2017. Overview of the Ca–Cu looping process for hydrogen production and/or power generation. Curr. Opin. Chem. Eng. 17, 1–8. https://doi.org/10.1016/j.coche.2017.04.010

Fernández, J.R., Abanades, J.C., 2017. Optimized design and operation strategy of a Ca Cu chemical looping process for hydrogen production. Chem. Eng. Sci. 166, 144–160. https://doi.org/10.1016/j.ces.2017.03.039

Fernandez, J.R., Abanades, J.C., Murillo, R., 2012. Modeling of sorption enhanced steam methane reforming in an adiabatic fixed bed reactor. Chem. Eng. Sci. 84, 1–11. https://doi.org/10.1016/j.ces.2012.07.039

Fernández, J.R., Abanades, J.C., Murillo, R., Grasa, G., 2012. Conceptual design of a hydrogen production process from natural gas with CO2 capture using a Ca–Cu chemical loop. Int. J. Greenh. Gas Control 6, 126–141. https://doi.org/10.1016/j.ijggc.2011.11.014

Fernández, J.R., Alarcón, J.M., Abanades, J.C., 2018. Study of the calcination of CaCO 3 by means of a Cu/CuO chemical loop using methane as fuel gas. Catal. Today. https://doi.org/10.1016/j.cattod.2018.02.053

Fouad, O.A., Hassan, A.M., Abd El-Wahab, H., Mohy Eldin, A., Naser, A.-R.M., Wahba, O.A.G., 2012. Synthesis, characterization and application of some nanosized mixed metal oxides as high heat resistant pigments: Ca2CuO3, Ca3Co2O6, and NiSb2O6. J. Alloys Compd. 537, 165–170. https://doi.org/10.1016/j.jallcom.2012.05.078

Hess, C., ElHaes, H., Waske, A., Büchner, B., Sekar, C., Krabbes, G., Heidrich-Meisner, F., Brenig, W., 2007. Linear Temperature Dependence of the Magnetic Heat Conductivity in CaCu 2 O 3. Phys. Rev. Lett. 98, 027201. https://doi.org/10.1103/PhysRevLett.98.027201

Imtiaz, Q., Hosseini, D., Müller, C.R., 2013. Review of Oxygen Carriers for Chemical Looping with Oxygen Uncoupling (CLOU): Thermodynamics, Material Development, and Synthesis. Energy Technol. 1, 633–647. https://doi.org/10.1002/ente.201300099

Kalinkin, A.M., Balyakin, K.V., Kalinkina, E.V., 2012. Kinetic and thermodynamic patterns of CaZrO3 formation at sintering zirconium dioxide with calcium carbonate. Russ. J. Gen. Chem. 82, 1753–1760. https://doi.org/10.1134/S1070363212110011

Kazi, S.S., Aranda, A., di Felice, L., Meyer, J., Murillo, R., Grasa, G., 2017. Development of Cost Effective and High Performance Composite for CO2 Capture in Ca-Cu Looping Process. Energy Procedia 114, 211–219. https://doi.org/10.1016/j.egypro.2017.03.1163

Kierzkowska, A.M., Müller, C.R., 2013. Sol-Gel-Derived, Calcium-Based, Copper-Functionalised CO_2 Sorbents for an Integrated Chemical Looping Combustion-Calcium Looping CO_2 Capture Process. ChemPlusChem 78, 92–100. https://doi.org/10.1002/cplu.201200232

Kierzkowska, A.M., Müller, C.R., 2012. Development of calcium-based, copper-functionalised CO2 sorbents to integrate chemical looping combustion into calcium looping. Energy Environ. Sci. 5, 6061. https://doi.org/10.1039/c2ee03079a

Lee, S.-Y., Park, S.-J., 2015. A review on solid adsorbents for carbon dioxide capture. J. Ind. Eng. Chem. 23, 1–11. https://doi.org/10.1016/j.jiec.2014.09.001

Li, J., Zhang, H., Gao, Z., Fu, J., Ao, W., Dai, J., 2017a. CO2 Capture with Chemical Looping Combustion of Gaseous Fuels: An Overview. Energy Fuels 31, 3475–3524. https://doi.org/10.1021/acs.energyfuels.6b03204

Li, J., Zhang, H., Gao, Z., Fu, J., Ao, W., Dai, J., 2017b. CO_2 Capture with Chemical Looping Combustion of Gaseous Fuels: An Overview. Energy Fuels 31, 3475–3524. https://doi.org/10.1021/acs.energyfuels.6b03204

Lu, H., Khan, A., Pratsinis, S.E., Smirniotis, P.G., 2009. Flame-Made Durable Doped-CaO Nanosorbents for CO_2 Capture. Energy Fuels 23, 1093–1100. https://doi.org/10.1021/ef8007882

Luo, C., Zheng, Y., Xu, Y., Ding, H., Zheng, C., Qin, C., Feng, B., 2015. Cyclic CO2 capture characteristics of a pellet derived from sol-gel CaO powder with Ca12Al14O33 support. Korean J. Chem. Eng. 32, 934–938. https://doi.org/10.1007/s11814-014-0291-0

Lyon, R.K., Cole, J.A., 2000. Unmixed Combustion: An Alternative to Fire. Energy Environ. Res. Corp. 18 Mason Irvine CA 92618-2706 USA 13.

Ma, J., Mei, D., Peng, W., Tian, X., Ren, D., Zhao, H., 2019. On the high performance of a core-shell structured CaO-CuO/MgO@Al2O3 material in calcium looping integrated with chemical looping combustion (CaL-CLC). Chem. Eng. J. 368, 504–512. https://doi.org/10.1016/j.cej.2019.02.188

Manovic, V., Anthony, E.J., 2011. Integration of Calcium and Chemical Looping Combustion using Composite CaO/CuO-Based Materials. Environ. Sci. Technol. 45, 10750–10756. https://doi.org/10.1021/es202292c

Manovic, V., Wu, Y., He, I., Anthony, E.J., 2011. Core-in-Shell CaO/CuO-Based Composite for CO_2 Capture. Ind. Eng. Chem. Res. 50, 12384–12391. https://doi.org/10.1021/ie201427g

Martínez, I., Armaroli, D., Gazzani, M., Romano, M.C., 2017. Integration of the Ca–Cu Process in Ammonia Production Plants. Ind. Eng. Chem. Res. 56, 2526–2539. https://doi.org/10.1021/acs.iecr.6b04615

Martínez, I., Martini, M., Riva, L., Gallucci, F., Van Sint Annaland, M., Romano, M.C., 2019. Techno-economic analysis of a natural gas combined cycle integrated with a Ca-Cu looping process for low CO2 emission power production. Int. J. Greenh. Gas Control 81, 216–239. https://doi.org/10.1016/j.ijggc.2018.12.026

Martínez, I., Romano, M.C., Chiesa, P., Grasa, G., Murillo, R., 2013. Hydrogen production through sorption enhanced steam reforming of natural gas: Thermodynamic plant assessment. Int. J. Hydrog. Energy 38, 15180–15199. https://doi.org/10.1016/j.ijhydene.2013.09.062

Mattisson, T., Leion, H., Lyngfelt, A., 2009. Chemical-looping with oxygen uncoupling using CuO/ZrO2 with petroleum coke. Fuel 88, 683–690. https://doi.org/10.1016/j.fuel.2008.09.016

McCusker, L.B., Von Dreele, R.B., Cox, D.E., Louër, D., Scardi, P., 1999. Rietveld refinement guidelines. J. Appl. Crystallogr. 32, 36–50. https://doi.org/10.1107/S0021889898009856

Navarro, M.V., López, J.M., García, T., Grasa, G., Murillo, R., 2017. Catalyst evaluation for high-purity H2 production by sorption-enhanced steam-methane reforming coupled to a Ca/Cu process. J. Power Sources 363, 117–125. https://doi.org/10.1016/j.jpowsour.2017.07.075

P. Fennell, B. Anthony, 2015. Calcium and Chemical Looping Technology for Power Generation and Carbon Dioxide Capture. Woodhead Publishing (Elsevier), Cambridge, UK.

Pato-Doldán, B., Rosnes, M.H., Dietzel, P.D.C., 2017. An In-Depth Structural Study of the Carbon Dioxide Adsorption Process in the Porous Metal-Organic Frameworks CPO-27-M. ChemSusChem 10, 1710–1719. https://doi.org/10.1002/cssc.201601752

Qin, C., Feng, B., Yin, J., Ran, J., Zhang, L., Manovic, V., 2015. Matching of kinetics of $CaCO_3$ decomposition and CuO reduction with CH_4 in Ca–Cu chemical looping. Chem. Eng. J. 262, 665–675. https://doi.org/10.1016/j.cej.2014.10.030

Qin, C., Yin, J., Liu, W., An, H., Feng, B., 2012. Behavior of CaO/CuO Based Composite in a Combined Calcium and Copper Chemical Looping Process. Ind. Eng. Chem. Res. 120911135600000. https://doi.org/10.1021/ie300677s

Qin, C., Yin, J., Luo, C., An, H., Liu, W., Feng, B., 2013. Enhancing the performance of CaO/CuO based composite for CO2 capture in a combined Ca–Cu chemical looping process. Chem. Eng. J. 228, 75–86. https://doi.org/10.1016/j.cej.2013.04.115

Radfarnia, H.R., Iliuta, M.C., 2013. Metal oxide-stabilized calcium oxide CO2 sorbent for multicycle operation. Chem. Eng. J. 232, 280–289. https://doi.org/10.1016/j.cej.2013.07.049

Reddy, G.K., Quillin, S., Smirniotis, P., 2014. Influence of the Synthesis Method on the Structure and CO_2 Adsorption Properties of Ca/Zr Sorbents. Energy Fuels 28, 3292–3299. https://doi.org/10.1021/ef402573u

Rietveld, H.M., 1969. A profile refinement method for nuclear and magnetic structures. J. Appl. Crystallogr. 2, 65–71. https://doi.org/10.1107/S0021889869006558

Shokrollahi Yancheshmeh, M., Radfarnia, H.R., Iliuta, M.C., 2016. High temperature CO2 sorbents and their application for hydrogen production by sorption enhanced steam reforming process. Chem. Eng. J. 283, 420–444. https://doi.org/10.1016/j.cej.2015.06.060

Thompson, P., Cox, D.E., Hastings, J.B., 1987. Rietveld Refinement of Debye-Scherrer Synchrotron X-ray Data from A1203 5.

Toby, B.H., 2006. *R* factors in Rietveld analysis: How good is good enough? Powder Diffr. 21, 67–70. https://doi.org/10.1154/1.2179804

Valverde, J.M., 2013. Ca-based synthetic materials with enhanced CO2 capture efficiency. J. Mater. Chem. A 1, 447–468. https://doi.org/10.1039/c2ta00096b

Valverde, J.M., Medina, S., 2015. Crystallographic transformation of limestone during calcination under CO_2. Phys. Chem. Chem. Phys. 17, 21912–21926. https://doi.org/10.1039/C5CP02715B

Vieira, R.B., Pastore, H.O., 2014. Polyethylenimine-Magadiite Layered Silicate Sorbent for CO_2 Capture. Environ. Sci. Technol. 48, 2472–2480. https://doi.org/10.1021/es404501e

Wang, C., Zhou, X., Jia, L., Tan, Y., 2014. Sintering of Limestone in Calcination/Carbonation Cycles. Ind. Eng. Chem. Res. 53, 16235–16244. https://doi.org/10.1021/ie502069d

Wang, J., Manovic, V., Wu, Y., Anthony, E.J., 2010. A study on the activity of CaO-based sorbents for capturing CO2 in clean energy processes. Appl. Energy 87, 1453–1458. https://doi.org/10.1016/j.apenergy.2009.08.010

Wang, K., Yu, Q., Duan, W., Qin, Q., Xie, H., 2014. The adaptability of Cu/Zr oxides as oxygen carrier used for chemical looping air separation (CLAS). J. Therm. Anal. Calorim. 115, 1163–1172. https://doi.org/10.1007/s10973-013-3440-5

Wang, M., Liu, J., Hu, J., Liu, F., 2015. O_2 –CO_2 Mixed Gas Production Using a Zr-Doped Cu-Based Oxygen Carrier. Ind. Eng. Chem. Res. 54, 9805–9812. https://doi.org/10.1021/acs.iecr.5b01944

Westbye, A., Aranda, A., Dietzel, P.D.C., Di Felice, L., 2018. The effect of Copper(II) oxide loading and precursor on the cyclic stability of combined mayenite based materials for calcium copper looping technology. Int. J. Hydrog. Energy. https://doi.org/10.1016/j.ijhydene.2018.11.200

Xiao, Q., Liu, Y., Zhong, Y., Zhu, W., 2011. A citrate sol–gel method to synthesize Li2ZrO3 nanocrystals with improved CO2 capture properties. J. Mater. Chem. 21, 3838. https://doi.org/10.1039/c0jm03243c

Zhai, Y., Ji, Y., Wang, G., Zhu, Y., Liu, H., Zhong, Z., Su, F., 2015. Controllable wet synthesis of multicomponent copper-based catalysts for Rochow reaction. RSC Adv. 5, 73011–73019. https://doi.org/10.1039/C5RA10999J

Zhao, M., Bilton, M., Brown, A.P., Cunliffe, A.M., Dvininov, E., Dupont, V., Comyn, T.P., Milne, S.J., 2014. Durability of CaO–$CaZrO_3$ Sorbents for High-Temperature CO_2 Capture Prepared by a Wet Chemical Method. Energy Fuels 28, 1275–1283. https://doi.org/10.1021/ef4020845

Zhou, R., Yu, T., Jiang, X., Chen, F., Zheng, X., 1999. Temperature-programmed reduction and temperature-programmed desorption studies of CuOrZrO2 catalysts 8.

Zhou, Z., Qi, Y., Xie, M., Cheng, Z., Yuan, W., 2012. Synthesis of CaO-based sorbents through incorporation of alumina/aluminate and their CO2 capture performance. Chem. Eng. Sci. 74, 172–180. https://doi.org/10.1016/j.ces.2012.02.042